Theor Appl Climatol (2013) 113:671–682
DOI 10.1007/s00704-012-0816-6

ORIGINAL PAPER

Temperature lapse rate in complex mountain terrain on the southern slope of the central Himalayas

D. B. Kattel · T. Yao · K. Yang · L. Tian · G. Yang · D. Joswiak

Received: 3 April 2012 / Accepted: 26 November 2012 / Published online: 12 December 2012

Abstract This study presents the first results of monthly, seasonal and annual characteristics of temperature lapse rate on the southern slope of the central Himalayas, based on 20 years record of surface air temperature at 56 stations in Nepal. These stations are located at a range of elevations between 72 and 3,920 m above sea level. It is proven that the lapse rate can be calculated with a linear regression model. The annual cycle of temperature lapse rate exhibits a bi-modal pattern: two maxima in the pre- and post-monsoon seasons respectively separated by two minima in winter and summer, respectively. This pattern is different from the findings from the other mountain regions and suggests different controlling factors in the individual seasons. The highest temperature lapse rate occurs in the pre-monsoon and is associated with strong dry convection (i.e., corresponding to the clear weather season and considerable sensible heat flux). The post-monsoon has the second highest lapse rate, and its cause is similar to the pre-monsoon season but with a relatively small thermal forcing effect after the rainy summer. The lowest lapse rate occurs in winter and is associated with strong radiative cooling and cold air flows over low-elevation areas. The summer lapse rate minimum is due to latent heating over the higher elevations and reduced solar heating over the lower elevations.

D. B. Kattel (✉) · T. Yao · K. Yang · L. Tian · G. Yang · D. Joswiak
Key Laboratory of Tibetan Environment Changes and Land Surface Processes, Institute of Tibetan Plateau Research, Chinese Academy of Sciences, P.O. Box 2871, 4A Datun Road, Chaoyang District,
Beijing 100101, China
e-mail: katteldb@gmail.com

D. B. Kattel
e-mail: katteldb@itpcas.ac.cn

T. Yao
e-mail: tdyao@itpcas.ac.cn

D. B. Kattel
University of Chinese Academy of Sciences, Beijing 100049, China

1 Introduction

Fundamentally, surface air temperature decreases with increasing elevation. This decrease in temperature with increasing elevation is widely known as the temperature lapse rate hereafter referred to as TLR. TLR is one of the most important characteristics of local and regional climates. Many studies (Laughlin 1982; Thyer 1985; Barry 2002; Pepin 2001; Rolland 2003; Tang and Fang 2006; Marshall et al. 2007; Blandford et al. 2008; Gardner et al. 2009; Gouvas et al. 2011) have reported that the TLR changes with macro-topography. They also suggested that its magnitudes vary in different locations as a function of energy balance regimes, such as surface condition, elevation, air moisture content, wind speed, cloudiness, radiative conditions, and distance from the sea.

Many researchers (Diaz and Bradley 1997; Barry 2002; Pepin 2001; Rolland 2003; Tang and Fang 2006; Mokhov and Akperov 2006; Marshall et al. 2007; Blandford et al. 2008; Minder et al. 2010) have emphasized the significance of the surface air temperature lapse rate in determining temperature range in many fields, such as glaciology, hydrology, ecology, forestry, and agriculture.

Numerous studies have been carried out on the annual cycle of surface air TLR and its controlling factors in many mountain regions. Relevant examples are studies of Minder et al. (2010) in the Washington Cascades Mountain, Rolland (2003) in Northern Italy and the Austrian Alps, Tang and Fang (2006) for northern and southern slopes of the Mt Taibai (China), Blandford et al. (2008) in South Central Idaho, Gouvas et al. (2011) in Greece, Diaz and Bradley (1997) in 40° N in the Northern Hemisphere, Pepin and

Losleben (2002) in the Colorado Rocky Mountains, and Harlow et al. (2004) in semiarid southeastern Arizona.

The Himalayas and Tibetan Plateau have complex terrain, and several studies suggest that this region strongly affects the onset and the intensity of Asia's monsoon through dynamic and thermal processes (Flohn 1957, 1968; Ye and Gao 1979; Wu and Zhang 1998; Shrestha et al. 2000; Ichiyanagi et al. 2007; Shrestha and Aryal 2010). In particular, the glaciological and hydrological cycles in this region are sensitive to regional temperature changes (Yao et al. 2006; Yang et al. 2011). Most relevant studies undertaken to date have focused on the Tibetan Plateau and the northern slopes of the Himalayas, whereas studies of the mountainous region on the southern slope of the Himalayas are very limited, perhaps due to a lack of meteorological record data. Using observed data series from 15 stations in the western part of Nepal (detailed information relating to elevation and the time periods used are not mentioned), Thyer (1985) briefly discussed the annual temperature gradient pattern, which revealed one minimum in winter, an increase towards spring, and another minimum in the summer months. However, detailed, systematic studies on the temperature lapse rates and their controlling factors in Nepal are still lacking.

The main objective of this study is to examine the monthly, seasonal, and annual characteristics of temperature lapse rate on the southern slope of the central Himalayas. In addition, the topographic influences on the variability of TLR magnitudes are also examined. As far as the authors are aware, this is the first attempt to examine the maximum, minimum, and mean temperature lapse rates in this region.

2 Data and methods

2.1 Site description and climatology

Nepal is situated within latitudes ordinarily defined as the subtropics and contains complex mountain terrain located on the southern slope of the central Himalayas (Fig. 1). The country is located between the latitudes of 26°22′ and 30° 27′ N and longitudes 80°04′ and 88°12′ E. Its shape is roughly rectangular and is orientated nearly parallel to the axis of the Himalayas (Fig. 1). The east-west length of the country is about 800 km and the average north-south width is approximately 200 km. Elevation ranges between a few tens of meters above sea level and 8,848 m.

The unique feature of Nepal is the existence of the tropical to alpine climate over a relatively south-north distance. The month of June records the highest mean temperature (25.4 °C), while May (30.4 °C) and July (21.1 °C) have the highest temperature for the maximum and minimum temperatures, respectively. Following the summer, the temperature starts decreasing from October and is lowest in January (figure not shown). The marked altitudinal range of the country has resulted in significant spatial variation of temperature (Shrestha and Aryal 2010).

The climate of Nepal during the summer is dominated by the southeasterly (moisture-laden air mass) monsoon (June–September) that provides most of the precipitation during this period (Kansakar et al. 2004; Shrestha and Aryal 2010). The distribution of this rainfall is strongly controlled by orography, with the foothill slopes of the Himalayas receiving some of the heaviest rain (Shrestha 2000; Lang and Barros 2002; Ichiyanagi et al. 2007). The spatial distribution of seasonal rainfall (total in cm) on the southern slope of the central Himalayas is presented in Fig. 2. The heaviest rainfall occurs in July (20-year monthly mean for 56 recording stations, 47.83 cm) and the lowest in November (20-year monthly mean, 0.99 cm).

Shrestha et al. (2000) found a significant relationship between Nepal's rainfall and the Southern Oscillation Index, as well as evidence for the modulation of rainfall totals by terrain. In general, the onset and the retreat of the southeasterly monsoon are associated with the change in the direction of seasonal winds and the northward and southward shift of the Inter Tropical Convergence Zone (Shrestha and Aryal 2010). The monsoon airflows over the Himalayas include the southerly winds that are forced to ascent from the Bay of Bengal and are enhanced by the cloud development with latent heat released over the Tibetan Plateau (Ueno et al. 2008).

During the winter and pre-monsoon months, other patterns emerge. In particular, rain and snowfall are associated with western disturbances as the prominent, synoptic weather systems move eastwards across the Himalayas (Shrestha 2000; Dimri 2007; Shrestha and Aryal 2010). In general, western disturbances are low-pressure synoptic systems that originate over the Mediterranean Sea or mid-Atlantic Ocean and travel eastward, driven by westerly winds at altitude (Dimri 2007). They dominate from November to March (Shrestha et al. 2000). The winter precipitation (see Fig. 2) is crucial to the mass balance of glaciers, particularly in the western part of the central Himalayas (Shrestha and Aryal 2010). The pre-monsoon season (March–May) is characterized by hot, dry weather with scattered rainfall associated with moderate to strong westerly winds. Towards the end of this period, the weather becomes more humid with thunderstorms (Kansakar et al. 2004). In the post-monsoon period, the rainfall activity is substantially reduced, with November typically being the driest month.

2.2 Data

Monthly mean maximum and minimum temperature and rainfall data from 56 (out of 66) stations covering the period 1985 to 2004 on the southern slope of the central Himalayas

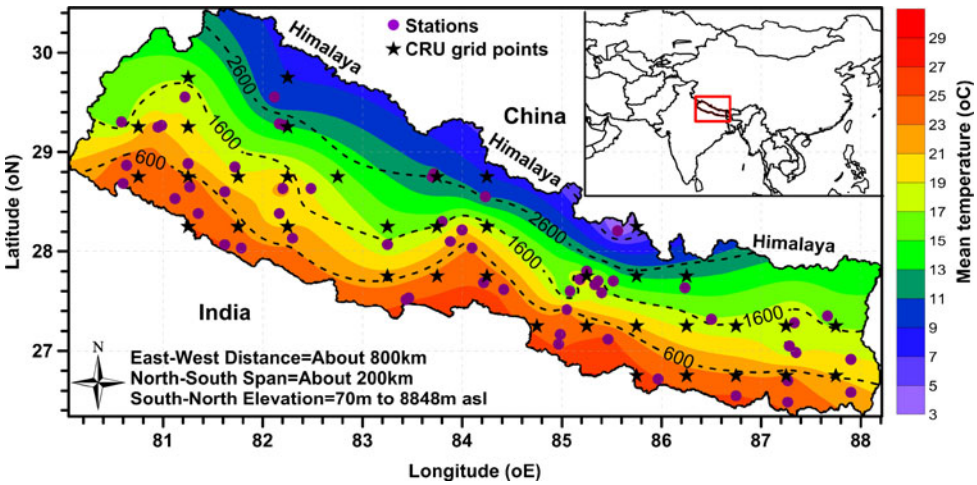

Fig. 1 Study area and spatial distribution of stations, mean temperature, and elevation on the southern slope of the central Himalayas. *Dashed lines* indicate elevation contours

were collected from the Department of Hydrology and Meteorology, Government of Nepal. Data cover an elevation range from 72 masl in the south to 3,920 masl in the north (Fig. 1). The names of the stations, elevation, and geographic information are presented in Table 1.

As a preliminary quality control, the 66 stations maximum and minimum temperature data series were manually inspected. Any suspicious values, for example a maximum temperature value that is lower than the corresponding minimum temperature value, were removed. Outliers were identified through Grubbs' methods (Grubbs 1950, 1969) using the statistical software package "Minitab." Grubbs' test is used to detect a single outlier in a univariate data set following a relatively normal distribution. Out of 26,880 (56×12×2×20) data values, 165 outliers were detected. Test statistics (T-S) were used as a filter to determine whether these values are outlier or true values. The test statistic (also known as *z*-score) was derived by dividing the difference between the mean and the individual value by the standard deviation. It was found that a higher proportion (115) of T-S values for most of the station lie between the ranges of 3 to 5. In addition, the detected values are ±2 °C different from the 20-year mean. Those values (remaining 50) for which test statistics were >5 and observed value that exceeded ±2 °C from the mean value were removed from the data set.

In order to ascertain whether the data series are homogeneous or not, a homogeneity test with respect to time was performed. Four different tests were performed, including Pettit's, Standard Normal Homogeneity Test, and Buishand's and Von Neumann's tests. The statistical software package

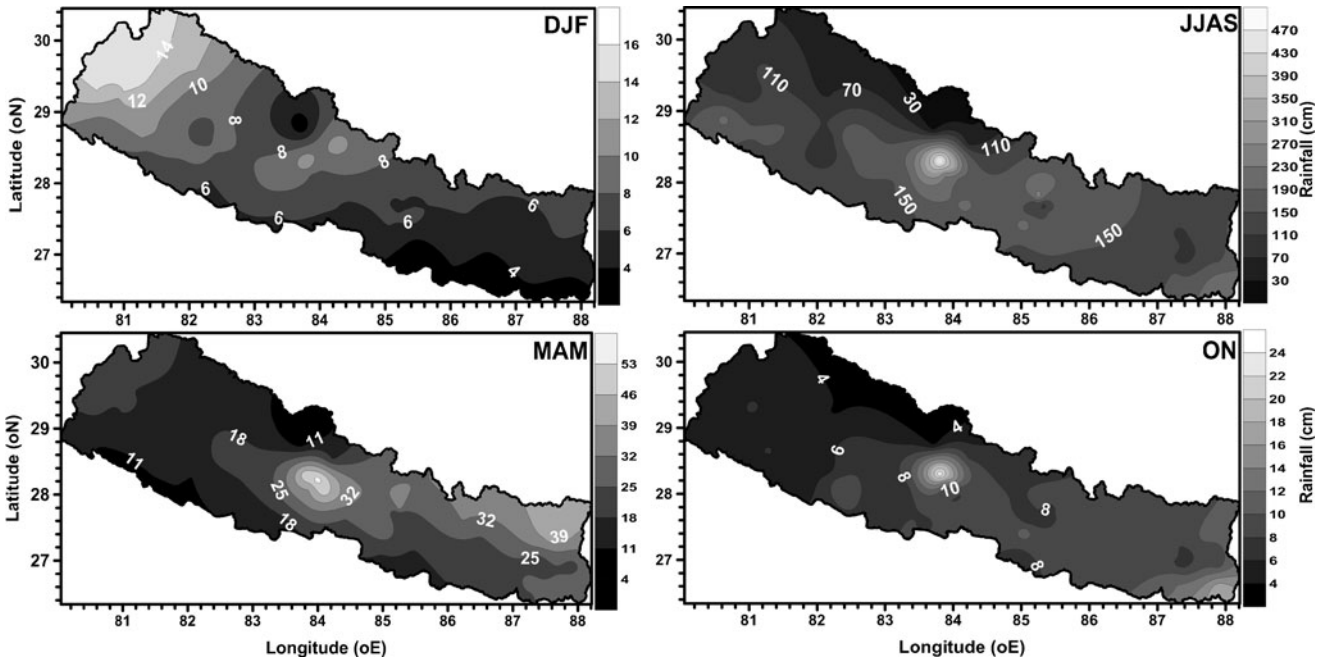

Fig. 2 Spatial distribution of total rainfall by season on the southern slope of the central Himalayas

Table 1 Descriptive information of the observational stations used in this study

Index No.	Station name	Longitude (deg E)	Latitude (deg N)	Elevation (masl)	Topography
104	Dadeldhura	80.58	29.30	1,848	Hilltop
202	Chainpur (West)	81.22	29.55	1,304	Valley (S)
203	Silgadhi Doti	80.98	29.27	1,360	Slope (S)
207	Tikapur	81.12	28.53	140	Flat (TAR)
209	Dhanghadi	80.60	28.68	170	Flat (TAR)
215	Godavari (West)	80.63	28.87	288	Flat (SW)
218	Dipayal (Doti)	80.95	29.25	617	Basin (R)
303	Jumla	82.17	29.28	2,300	Valley (S)
307	Rara	82.12	29.55	3,048	Slope (S)
310	Dipal Gaun	82.22	29.27	2,310	Valley (N)
401	Pusma Camp	81.25	28.88	950	Hilltop
402	Dailekh	81.72	28.85	1,402	Slope (N)
405	Chisapani (Karnali)	81.27	28.65	225	Basin (R)
406	Surkhet	81.62	28.60	720	Valley(SW)
416	Nepalgunj	81.62	28.07	144	Flat (TAR)
417	Rani Jaruwa Nur	81.35	28.38	200	Flat (TAR)
419	Sikta	81.78	28.03	195	Flat (TAR)
446.1	Kynjing	85.56	28.21	3,920	Valley (N)
508	Tulsipur	82.30	28.13	725	Flat (SW)
511	Salyan Bazar	82.17	28.38	1,457	Valley (N)
513	Chaur Jhari Tar	82.20	28.63	910	Flat (M)
601	Jomsom	83.72	28.78	2,744	Slope (S)
604	Thakmarpha	83.70	28.75	2,566	Valley (N)
705	Bhairhawa airport	83.43	27.52	109	Flat (TAR)
706	Dumkauli	84.22	27.68	154	Flat (SW)
707	Bhairahwa	83.47	27.53	120	Flat (TAR)
725	Tamghas	83.25	28.07	1,530	Slope (S)
804	Pokhara airport	84.00	28.22	827	Flat (V)
805	Syangja	83.88	28.10	868	Basin (R)
814	Lumle	83.80	28.30	1,740	Slope (S)
815	Khairini Tar	84.10	28.03	500	Basin (R)
816	Chame	84.23	28.55	2,680	Valley (S)
902	Rampur	84.42	27.62	256	Flat (SW)
905	Daman	85.08	27.60	2,314	Hilltop
906	Hetunda	85.05	27.42	474	Flat (SW)
909	Simra airport	84.98	27.17	130	Flat (TAR)
911	Parwanipur	84.97	27.07	115	Flat (TAR)
1007	Kakani	85.25	27.80	2,064	Slope (S)
1022	Godavari	85.40	27.58	1,400	Valley(S)
1029	Khumaltar	85.33	27.67	1,350	Valley (C)
1030	Kathmandu airport	85.37	27.70	1,336	Valley (C)
1038	Dhunibesi	85.18	27.72	1,085	Flat (M)
1043	Nagarkot	85.52	27.70	2,163	Slope (N)
1103	Jiri	86.23	27.63	2,003	Valley (S)
1111	Janakpur airport	85.97	26.72	90	Flat (TAR)
1121	Karmaiya	85.47	27.12	131	Flat (SW)
1206	Okhaldhnga	86.50	27.32	1,720	Hilltop
1223	Rajbiraj	86.75	26.55	91	Flat (TAR)
1303	Chainpur (East)	87.33	27.28	1,329	Hilltop

Table 1 (continued)

Index No.	Station name	Longitude (deg E)	Latitude (deg N)	Elevation (masl)	Topography
1304	Pakhribas	87.28	27.05	1,680	Slope (S)
1307	Dhankuta	87.35	26.98	1,210	Slope (S)
1319	Biratnagar airport	87.27	26.48	72	Flat (TAR)
1320	Tarahara	87.27	26.70	200	Flat (TAR)
1405	Taplejung	87.67	27.35	1,732	Slope (S)
1407	Ilam Tea Estate	87.90	26.92	1,300	Hilltop
1421	Gaida	87.90	26.58	143	Flat (TAR)

N North, *S* South, *C* central, *TAR* Terai region (plain area), *SW* Siwalik (outer Himalayas), *M* mountain region, *V* valley bottom

XLSTAT was used to obtain the results. The p values were computed using 1,000 Monte Carlo simulations. As the computed p value is higher than the significance level alpha (0.01 and 0.05), the null hypothesis H_o (that the data are homogeneous) cannot be rejected. The 56 stations with significance values in excess of 0.01 are used in the analysis. Ten stations out of 66 failed the homogeneity tests ($p<0.001$) and were therefore not included in the analysis. Finally, a normality test was performed on the 56 data series. The Shapiro–Wilk, Lilliefors Probability, and Kolmogorov–Smirnov tests show that the data series are normally distributed.

Annual and seasonal means were calculated for all stations using the arithmetic mean method. The four seasons are divided into winter (December, January, and February), pre-monsoon (March–May), monsoon (June–September), and post-monsoon (October and November). The annual mean is averaged over January–December, and monthly mean average is the mean of monthly maximum and minimum temperature. Monthly, seasonal, and annual 20-year means of each station were calculated to evaluate TLR.

In order to investigate the relationship with the annual TLR cycle, the monthly mean rainfall over the region was also calculated using the 20-year data series from 56 observational stations.

The annual cycle of temperature lapse rate was also compared with cloud cover. The Climate Research Unit (CRU) TS 3.10 monthly cloud cover data (land) between 1985 and 2004 were obtained from the CRU website (http://climexp.knmi.nl/). The cloud cover data are distributed in $0.5^{\circ} \times 0.5^{\circ}$ grid squares. The nearest 37 grid points to the 56 observational stations were selected to compute the mean value. The spatial distribution of CRU TS 3.10 data grid points is presented in Fig. 1.

2.3 Topographic classifications

The 56 stations are distributed across Nepal within a wide range of terrain types. Based on the location type, stations were classified into five zones (flat terrain, valley, river basin, sloping ground, and hilltop) through subjective visual comparison with elevation from SRTM3 digital elevation data (USGS http://earthexplorer.usgs.gov/). Coordination and projection of the digital elevation model are according to the WGS-1984-UTM-Zone 43 N. The grid resolution of DEM data is 90 m. Twenty-two of the 56 stations are located in relatively flat areas (Table 1). The elevation of these stations ranges between 72 and 1,000 masl. Of the 34 remaining stations, 13 are located in valleys, 11 on sloping ground, 4 are located in the surrounding of river basins, and 6 are on hilltops.

2.4 Determination of colinearity

In order to investigate the relationship between temperature and latitude, longitude, and elevation, multiple regression was performed. Multiple regression is a technique that allows additional factors to enter the analyses separately so that the effect of each can be estimated. In addition, it is valuable for quantifying the impact of various simultaneous influences upon a single dependent variable using the following equation:

$$T_{\mathrm{mno}} = i_{\mathrm{mno}}\mathrm{Lat} + j_{\mathrm{mno}}\mathrm{Lon} + \mathrm{k_{mno}E} + \mathrm{D_{mno}} + \mathrm{e} \quad (1)$$

In Eq. (1), T (temperature in degree Celsius) is the dependent variable, Lat (latitude in degree N), Lon (longitude in degree E), and E (elevation in kilometers) are the independent variables, and D and e are the constant and error of multiple regression terms, respectively. The letters "i, j, and k" represent the coefficients from the multiple regression, and "m, n, and o" are the maximum, minimum, and mean temperatures, respectively.

2.5 Lapse rate estimation

Maximum, minimum, and mean temperatures demonstrate a direct relationship with elevation based on the multicolinearity analyses (discussed in Section 3). Thus, a temperature–elevation relationship is established using a simple

linear regression method, which was widely adopted by previous studies in other mountain regions (Thyer 1985; Rolland 2003; Harlow et al. 2004; Mokhov and Akperov 2006; Blandford et al. 2008; Minder et al. 2010). Therefore, the series of linear equations were obtained from the following formula:

$$T_{\mathrm{mno}} = C_{\mathrm{mno}} - \mathrm{LR}_{\mathrm{mno}} \times \mathrm{E} + \mathrm{e} \quad (2)$$

In Eq. (2), T (temperature in degree Celsius) is the dependent variable, and E (elevation in kilometers) is the independent variable, and C and e are the constant for temperature in degree Celsius at zero elevation and error of regression terms, respectively. The coefficient –LR is the temperature lapse rate in degree Celsius per kilometer, and "m, n, and o" are the monthly maximum, minimum, and mean temperatures, respectively.

3 Results and discussion

3.1 Linear relationship

Multicolinearity analyses between surface air temperature and three independent variables (latitude, longitude, and elevation) revealed a direct relationship only with elevation. The highest standard errors were observed for latitude (max=0.69; min=0.95) and longitude (max=0.24; min=0.33), while the lowest were observed for the elevation (max=0.0003; min=0.0004). This result may be due to wide temperature and altitudinal variations within the same latitude and longitudinal belts (Fig. 1).

In addition, the highest values of variance inflation factor (VIF) were found for latitude (14.19, p=0.13) and longitude (12.13, p=0. 66) and the lowest for elevation (3.71, $p<$ 0.0001). Thus on the basis of VIF and larger probability value (>0.05), it is reasonable to eliminate the latitude and longitude variables. This result confirms that the temperature can be predicted with respect to elevation. Therefore, the temperature–elevation relationships were computed to determine the temperature lapse rate using Eq. (2). In order to determine the accuracy of the temperature lapse rate and the associated topographic influence, the correlation coefficient and regression errors were analyzed.

3.1.1 Analyses of correlation coefficients

The computed correlation coefficients between monthly temperature and elevation are presented in Table 2. The correlation coefficient between temperature and elevation shows a statistically significant inverse relationship ($p<$ 0.0001). The high correlation coefficients in the table suggest that an inverse linear relationship between temperature and elevation is applicable regardless of the fact that stations are spread out across a range of topography. Thus, the calculated TLR values in this study are suitable for examining monthly, seasonal and annual characteristics.

Figure 3 displays the monthly variation of the correlation coefficient (r). The correlation coefficients between maximum and mean temperature with elevation vary between −0.94 and −0.98. However, the correlation coefficient between minimum temperature and elevation is lower and more variable, ranging from −0.86 to −0.97. Gouvas et al. (2011) suggested that factors other than elevation influence minimum temperature, including humidity, cloudiness, wind velocity, the orientation of valleys, and the general drainage pattern of cold air flow from hilltops and higher ground.

Figure 3 shows decreasing correlation coefficients beginning in October and reaching a minimum in December (−0.86) and January (−0.87), which corresponds to the period of minimum temperature. Correlation coefficients increase in March and reach the highest values from May until September, ranging between −0.95 and −0.97. The lower correlation coefficients may be related to inversions that weaken the temperature-elevation relationship (Marshall et al. 2007). Inversions (the opposite effect of TLR) may set in when cold air sinks and displaces warmer air, especially at night (Rolland 2003). This phenomenon frequently occurs in valleys and at flat terrain. In contrast, the comparatively lower correlation coefficients between maximum summer temperature and elevation may be weaker due to the frequent terrain-dependent monsoon rainfall events.

3.1.2 Analyses of residual errors

The monthly correlation coefficient between temperature and elevation is comparatively lower for minimum and stronger for maximum temperature, excluding summer months. Lower (higher) correlation coefficients are found with higher (lower) residual regression errors. This result is consistent with previous results (e.g., Gouvas et al. 2011; Dobrowski et al. 2009) from other mountain regions. Harlow et al. (2004) and Gouvas et al. (2011) suggested that the local cloud conditions and topographic setting are possible factors for higher errors. The ranges of residual errors are higher for minimum temperature (3.1–5.2 °C) compared with maximum temperature (1.4–2.3 °C) during the non-monsoon months (Table 2). Highest residual errors for the regression of minimum temperature with elevation are observed in winter while the lowest values are observed in summer (Table 3). During the summer, higher residual errors for the regression of maximum temperature with elevation are found.

In order to investigate the topographic relationship, the seasonal value of residual errors from the regressions of each station was calculated. Means of each topographic subset were calculated for the analysis (Fig. 4). The residual errors are between ±3 °C for all seasons for the maximum

Table 2 Results of the regression between maximum, minimum, and mean temperature and elevation

Months	Maximum temperature					Minimum temperature					Mean temperature				
	C_m (°C)	LR_m (°C/km)	r	SE	RS	C_n (°C)	LR_n (°C/km)	r	SE	RS	C_o (°C)	LR_o (°C/km)	r	SE	RS
Jan	22.81	−4.5	−0.95	0.30	2.0	9.73	−4.1	−0.87	0.45	4.7	16.27	−4.3	−0.96	0.26	1.6
Feb	26.68	−5.7	−0.98	0.25	1.4	11.80	−4.4	−0.89	0.45	4.6	19.24	−5.0	−0.97	0.24	1.4
Mar	32.28	−6.4	−0.98	0.26	1.6	15.68	−4.6	−0.89	0.46	4.9	23.98	−5.5	−0.97	0.26	1.5
Apr	36.60	−6.8	−0.97	0.32	2.3	20.37	−5.3	−0.92	0.45	4.7	28.48	−6.1	−0.97	0.29	1.9
May	36.80	−6.2	−0.95	0.42	4.0	24.02	−5.7	−0.95	0.36	2.9	30.41	−6.0	−0.97	0.31	2.1
Jun	35.83	−5.4	−0.94	0.39	3.5	26.00	−5.3	−0.97	0.28	1.8	30.91	−5.4	−0.97	0.27	1.7
Jul	33.76	−4.7	−0.95	0.32	2.4	26.07	−4.8	−0.96	0.27	1.6	29.92	−4.7	−0.97	0.24	1.3
Aug	33.99	−4.9	−0.96	0.29	2.0	26.00	−4.8	−0.96	0.27	1.7	30.00	−4.8	−0.97	0.23	1.2
Sep	33.42	−5.0	−0.96	0.29	2.0	24.99	−5.1	−0.97	0.27	1.6	29.20	−5.0	−0.98	0.21	1.0
Oct	32.46	−5.4	−0.97	0.27	1.7	20.96	−5.3	−0.94	0.37	3.1	26.71	−5.4	−0.98	0.20	0.9
Nov	29.42	−5.4	−0.97	0.27	1.6	15.44	−4.7	−0.90	0.46	4.9	22.43	−5.1	−0.97	0.23	1.2
Dec	25.10	−4.8	−0.96	0.28	1.7	11.17	−4.1	−0.86	0.48	5.2	18.14	−4.5	−0.97	0.23	1.2

All regressions are statistically significant at $p<0.0001$

C_m maximum constant temperature at zero elevation, C_n minimum constant temperature at zero elevation, C_o mean constant temperature at zero elevation, LR_m lapse rate of maximum temperature, LR_n lapse rate of minimum temperature, LR_o lapse rate of mean temperature, r correlation coefficient, *SE* standard error of estimate for regression intercept, *RS* residual error of the regression

temperature and ±4 °C for the minimum temperature during non-monsoon seasons. The winter season has the highest residual error (±4 °C) for minimum temperature, while the summer season shows the lowest residual error value (±1 °C).

It is noted that in all seasons, the flat terrain and valley stations have negative residuals for the minimum temperatures (Fig. 4b). This result is likely due to the strong radiative cooling in the flat terrain and air drainage inversion at the valley bottoms. In similar geographic locations supporting the formation and maintenance of cold air pools, Dobrowski et al. (2009) also found negative residuals. They also concluded that the residuals increased with increasing clear sky irradiance. An inversion due to radiative cooling typically develops in calm air under clear skies over flat terrain and is often accompanied by the development of fog (Critchfield 2004). On the other hand, cold air from the hilltop and slope sites tends to flow downward and collect in valley bottoms, creating an inverted lapse rate on the slopes and in the free atmosphere over the valley floor. In the non-monsoon season, valley and river basin stations reveal positive residuals for the regression of maximum temperature with elevation (Fig. 4a). This result may be due to strong radiative heating during clear sky conditions.

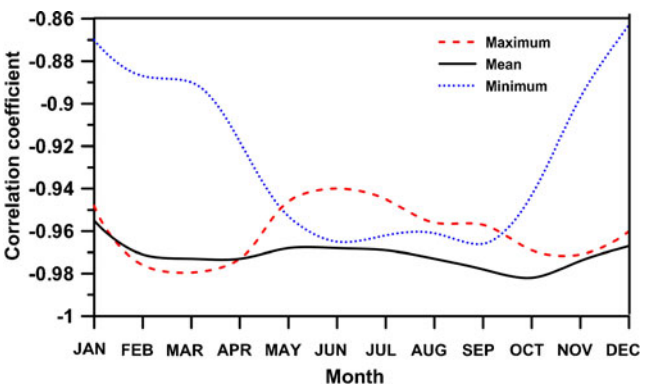

Fig. 3 The annual variability of correlation coefficient (r) obtained from the regression between temperature and elevation

It is also noted that all seasons exhibit positive residuals for the hilltop and sloping ground stations, particularly for minimum temperature (Fig. 4b). The high temperature at the hilltop and slope stations at night may be associated with an inverted lapse rate due to the inversion effect. However, the opposite effect is seen for maximum temperature at the hilltop and slopes during all seasons (Fig 4a), probably as a result of cloud formation during the day. It is noted that, due to a lack of sufficient data, this study does not differentiate between exposure and aspect effects.

3.2 Temperature lapse rate

In this study, increasingly negative TLRs, compared with the seasonal value, are considered as the higher decrease of temperature with increasing elevation, while the less negative values are considered as the temperature inversion. Table 2 shows that the lapse rate during maximum temperatures is higher than that for minimum temperatures for all months except June to October. This is due to the adiabatic

Table 3 Results of the regression between annual and seasonal mean temperature and elevation

Period	Parameter	Symbol	C (°C)	LR (°C/km)	r	r^2 (%)	SE	RS
Annual	Maximum	m	31.59	−5.4	−0.97	94	0.26	1.6
	Minimum	n	19.57	−4.9	−0.96	92	0.28	2.5
	Mean	o	25.58	−5.2	−0.99	97	0.18	0.9
Pre-monsoon (MAM)	Maximum	m	35.20	−6.5	−0.97	94	0.31	2.2
	Minimum	n	20.25	−5.3	−0.94	89	0.37	3.1
	Mean	o	27.72	−5.9	−0.98	96	0.24	1.3
Summer (JJAS)	Maximum	m	34.26	−5.0	−0.95	91	0.32	2.3
	Minimum	n	26.03	−5.1	−0.99	97	0.16	0.6
	Mean	o	30.15	−5.1	−0.98	96	0.20	0.9
Post-monsoon (ON)	Maximum	m	30.97	−5.4	−0.97	94	0.26	1.6
	Minimum	n	18.43	−5.2	−0.94	88	0.38	3.3
	Mean	o	24.71	−5.3	−0.98	97	0.19	0.9
Winter (DJF)	Maximum	m	24.88	−5.0	−0.97	94	0.26	1.5
	Minimum	n	11.05	−4.3	−0.89	78	0.44	4.5
	Mean	o	17.97	−4.7	−0.97	94	0.24	1.3

All regressions are statistically significant at $p<0.0001$. Symbols are identical to those in Table 2

MAM March, April, and May, *JJAS* June, July, August, and September, *ON* October and November, *DJF* December, January, and February

mixing within the boundary layer in the daytime. The mean TLRs vary from −4.3 °Ckm^{-1} (r^2=91 %) in January to −6.1 °C km^{-1} (r^2=95 %) in April (Table 2). The lapse rate during maximum temperature has the highest value of −6.8 °C km^{-1} (r^2=95 %) in April and the lowest value of −4.5 °Ckm^{-1} (r^2=90 %) in January. In contrast, the lapse rate for minimum temperatures range from −4.1 °Ckm^{-1} in December and January (r^2=75 and 76 %, respectively) to −5.7 °Ckm^{-1} (r^2=91 %) in May.

The annual mean TLR on the southern slope of the central Himalayas (Table 3) is −5.2 °Ckm^{-1} (r^2=97 %), which is −1.3 °Ckm^{-1} lower than the free-air moist adiabatic lapse rate (−6.5 °Ckm^{-1}) (Barry and Chorley 2003). This result may be expected due to the dominance of moist convection in low latitudes (0–25° N), where the lapse rate typically agrees well with the moist adiabatic lapse rate (Stone and Carlson 1979). Our annual mean TLR value of is consistent with the result of Devkota (2004) (−5.2 °Ckm^{-1}). In addition,

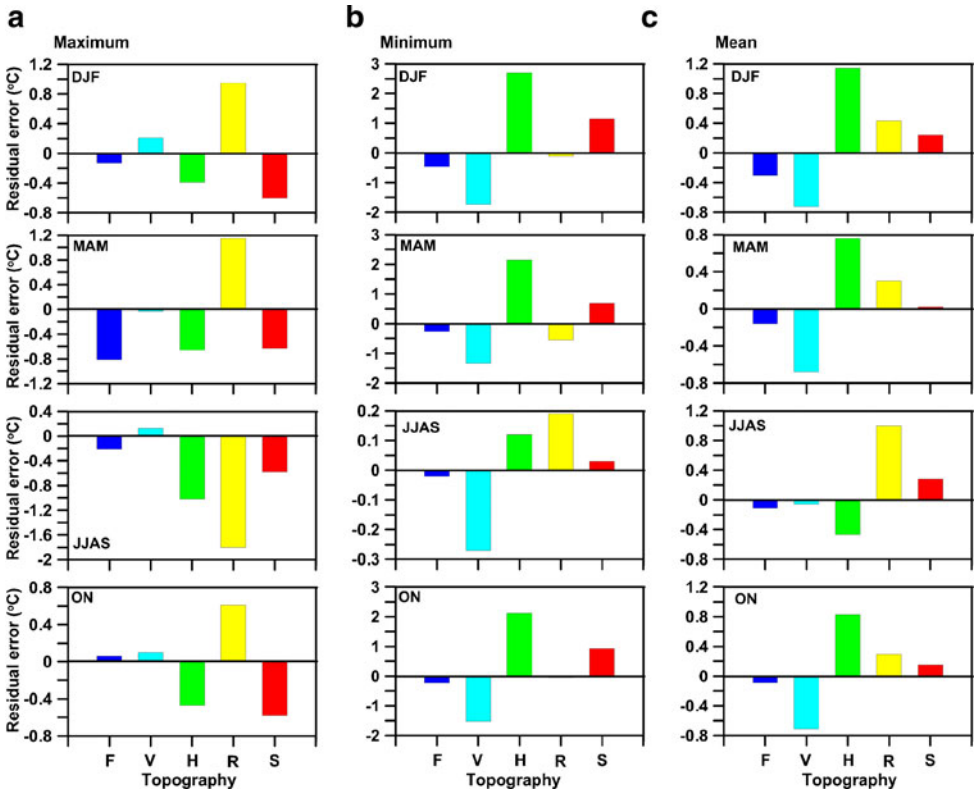

Fig. 4 The mean of the maximum (**a**), minimum (**b**), and mean (**c**) residual error of the regression with five different topographic locations, including flat terrain (*F*), valley (*V*), Hilltop (*H*), river basin (*R*), and sloping ground (*S*)

the annual mean TLR value is −0.1 °Ckm^{-1} higher than in western Nepal (Thyer 1985). The annual mean maximum TLR on the southern slope of the central Himalayas (Table 3) is higher (−5.4 °Ckm^{-1}, r^2=94 %) than the annual mean minimum TLR (−4.9 °Ckm^{-1}, r^2=92 %).

The annual cycle of TLR for maximum, minimum, and mean temperatures on the southern slope of the central Himalayas is presented in Fig. 5. The seasonal variations of TLRs exhibit bi-modal patterns. There are two TLR peaks in both the pre-monsoon and the post-monsoon periods, and two lowest values occur in the winter and the monsoon period, respectively (Fig. 5). The bi-modal pattern of TLR variability is distinct from other mountain regions in the USA (south-central Idaho, Washington Cascades, Colorado Rocky Mountains, and semi-arid southeastern Arizona) in Europe (Northern Italy, Greece, and the Austrian Alps) and in China (northern and southern slope of Mt. Taibai). Previous studies in those regions have reported lower lapse rates in winter and higher lapse rates in summer due to the maximum dry convection in summer and minimum in winter due to temperature inversions (Diaz and Bradley 1997; Pepin and Losleben 2002; Rolland 2003; Richardson et al. 2004; Harlow et al. 2004; Tang and Fang 2006; Marshall et al. 2007; Blandford et al. 2008; Gardner et al. 2009; Minder et al. 2010).

The TLR variability is mainly controlled by the topography and climatology of the region. Many previous studies have suggested that the TLR magnitude may depend on latitude, surface condition, elevation, moisture level, wind speed, cloudiness, distance from the sea, and the slope and aspect effect on solar insolation (Stone and Carlson 1979; Thyer 1985; Pepin 2001; Barry and Chorley 2003; Rolland 2003; Tang and Fang 2006; Marshall et al. 2007; Blandford et al. 2008; Gardner et al. 2009; Gouvas et al. 2011).

We note that the majority of the previously mentioned study regions are located in mid-latitude mountain systems, where there is no distinct summer wet season or where winter is the wettest season. Our study region is intermediate between the mid-latitudes and the tropics, and the regional climate is strongly dominated by two synoptic weather systems (e.g., southeasterlies in summer and westerlies in winter). The distinct bi-modal TLR patterns observed in this region may be associated with differing climatic and topographic regimes. The possible controlling factors on the TLR are discussed further in Section 3.3.

3.3 Controlling factors on the temperature lapse rate

The distinction between wet and dry conditions is extremely important in controlling lapse rates near the surface. In this study, we examine the relationship between TLR with rainfall, cloud cover, and the saturation vapor pressure (e_s) lapse rate. The saturation vapor pressure is a function of temperature and can be calculated using the well-known formula of Tetens (1930), which is based on the Clausius–Claperon relationship. The e_s lapse rate in this study is calculated using the linear regression method between calculated saturation vapor pressure at individual stations and elevation. The annual cycle of 20-year monthly mean rainfall and cloud cover on the southern slope of the central Himalayas is presented in Fig. 6. The annual cycle of maximum, minimum and mean e_s lapse rate is presented in Fig. 7.

There is a similar pattern of fluctuation between monthly rainfall and cloud cover in the annual variability (Fig. 6), and their relationship is robust (r=0.97, p<0.001). The highest cloud cover (>55 %) and rainfall (>25 cm/month) occurs in the summer, and the lowest cloud cover and rainfall (<45 % and <5 cm/ month) occur between fall and spring. The mean e_s lapse rate has the lowest value (−3.5 hPa/km, r=−0.96, and p<0.0001) in January and highest (−9.7 hPa/km, r=−0.95, and p<0.0001) in May. The value remains nearly constant from July through September (Fig. 7).

The regression between mean TLR and rainfall shows a weak negative relationship (r=−0.17, r^2=0.03 %), suggesting that the fluctuations of lapse rate for some seasons are not consistently associated with rainfall. The bi-modal patterns of TLR in Fig. 5 and the sinusoidal pattern of rainfall

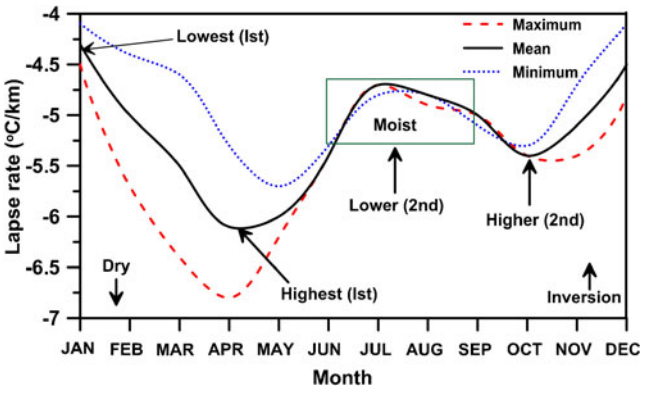

Fig. 5 Annual cycle of maximum (*dashed red line*), minimum (*dotted blue line*), and mean (*solid black line*) temperature lapse rates

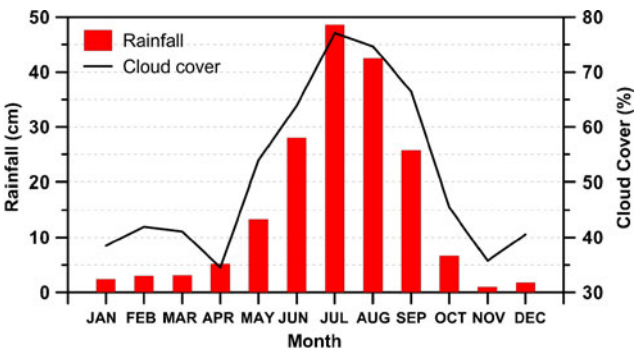

Fig. 6 Monthly means of CRU TS 3.10 cloud covered land (*solid black line*) and observed rainfall (*bars*) on the southern slope of the central Himalayas between 1985 and 2004

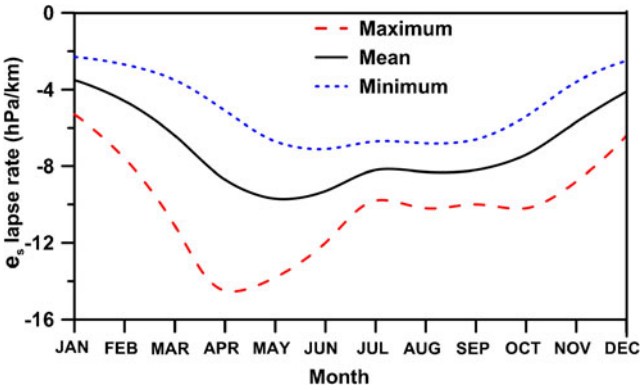

Fig. 7 Annual cycle of maximum (*dashed red line*), minimum (*dotted blue line*), and mean (*solid black line*) saturation vapor pressure (e_s) lapse rates on the southern slope of the central Himalayas

in Fig. 6 support this result. On the other hand, the correlation between mean TLR and e_s lapse rate exhibits a statistically significant, positive relationship (r=0.63, p<0.05), which indicates that the TLR fluctuation is consistently associated with the fluctuation of e_s lapse rate in all seasons. As actual vapor pressure (e) data are not available, further explanation of the seasonal TLR change is difficult.

TLR is lower in humid or cooler atmospheric conditions, and higher in dryer or warmer conditions (Pepin 2001; Tang and Fang 2006; Blandford et al. 2008; Gardner et al. 2009; Minder et al. 2010). The fluctuations in the annual cycle of TLR (Fig. 5) on the southern slope of the central Himalayas are in good agreement with these conclusions. In addition, the annual cycle of e_s lapse rate in Fig. 7 further supports the effect of dry and moist conditions in enhancing (in pre-monsoon season) and reducing (in monsoon season) regional TLR. Lowest TLRs are observed during the monsoon season. This is expected since the air over high elevations may be warmed by latent heat release associated with water vapor condensation, thereby reducing the lapse rate. Latent heat transfers depend on moisture content in the atmosphere (Marshall et al 2007). In response to heavy summer rainfall (Fig. 2), surface temperatures decrease and moist adiabatic processes prevail (Thyer 1985). Thus, the stable lapse rate for both maximum (−5.0 °Ckm^{-1}) and minimum (−5.1 °Ckm^{-1}) temperature in summer implies a strong association with rainfall amount.

Surface temperature oscillations also depend on cloudiness. The largest cloud cover occurs in the summer months and is lower in the non-monsoon months (Fig. 6). Significant cloud cover leads to a reduction in insolation during the day and a confinement of outgoing long-wave radiation during the night (Bhutiyani et al. 2007), thereby increasing minimum surface temperatures. Therefore, cloudy skies and moist conditions may reduce the daytime TLR value and enhance the nighttime TLR, minimizing the difference between the TLR associated with maximum and minimum temperatures. Topography may also play a role in reducing surface air temperature, particularly in the summer months during the day. The lower correlation coefficient in Fig. 3 and the highest residual error in Table 2 support this result. In addition, the plot of residual error (negative) in Fig. 4 also suggests that the flat terrain, river basin, hilltop, and sloping ground stations are relatively cooler during the day as compared with the night. This result may be associated with the occurrence of cloud cover during the day, which was previously reported by Kurosaki and Kimura (2002) for the monsoon.

In July, extensive cloud cover (77.08 %) occurs (Fig. 6). This month also has a lower mean TLR (−4.7 °Ckm^{-1}), which is −0.4 and−0.8 °Ckm^{-1} less than in November and April, respectively. The difference between the maximum and minimum TLR in summer is small (−0.1 °Ckm^{-1}). In November and April, low cloud cover (35.77 % in November and 34.56 % in April) occurs on the southern slope of the central Himalayas (Fig. 6), resulting in a higher TLR (Fig. 5). The peak in lapse rate during April is likely related to the vertical gradient of pre-monsoon snow cover (e.g., deep cover at high elevations, none at low elevations).

However, we cannot use the rainfall and cloud cover to account for the lowest mean TLR in winter (Table 3), when both cloud cover and rainfall are lowest (Fig. 6). The lowest mean TLR value occurring in winter implies other controlling factors play a more important role. During winter, skies are clear and radiative cooling is intense, leading to a stable stratification and producing a temperature inversion (Critchfield 2004). This condition facilitates the development of microclimates (Thyer 1985) and cold air deposition in low areas through down slope flow at the flat terrain and valleys. Foggy conditions may enhance the winter temperature inversion (Rolland 2003). Topography may also have a crucial role in enhancing the inversion effect, particularly in winter during the nighttime. The lowest correlation coefficient and the highest residual errors (Table 3), and the negative residual for the flat terrain and valley stations (Fig. 4) support this notion. In the winter, the highest positive residual in Fig. 4 suggests relatively warmer conditions at hilltop and sloping ground stations at night. This result may be due to the inverted lapse rate.

The pre-monsoon season, dominated by clear skies, has the highest mean TLR (Table 3) and the largest difference of lapse rate between maximum and minimum temperature. With the absence of clouds, land surfaces receive more incoming solar radiation compared with outgoing radiation, thereby raising daytime surface temperatures (Blandford et al. 2008). Large sensible heat flux is therefore expected, which can trigger strong dry convection in the daytime. This season also has the highest daytime e_s lapse rate (Fig. 7). As a result, the TLR for maximum temperatures reaches a maximum value in this season. On the other hand, outgoing

long wave radiation emitted under clear sky conditions cools the surface at night and therefore enhances the difference between daytime and nighttime TLRs.

The second TLR peak is observed in the post-monsoon season during October and November (Fig. 3). The magnitude of mean TLR in this season is lower compared with the pre-monsoon season but higher compared with the winter and summer seasons. The post-monsoon season also has the least difference between the maximum (−5.4 °Ckm^{-1}) and minimum (−5.2 °Ckm^{-1}) TLR (Table 3). Weather conditions during this time are similar to pre-monsoon conditions, but the thermal forcing effect is relatively small due to the disturbances between the phase of monsoon retreat and the onset of winter westerlies.

4 Conclusions

Based on the 1985 to 2004 climatology of surface air-temperature records from 56 stations in Nepal with an elevation range from 72 to 3,920 masl, the monthly, seasonal, and annual temperature lapse rates on the southern slope of the central Himalayas were analyzed. Temperature lapse rates were estimated with a linear regression model.

A unique feature of the temperature lapse rate along the southern slope of the central Himalayas is a bi-modal pattern in the annual cycle: two maxima in the pre- and post-monsoon seasons and two minima in the winter and summer seasons. This bi-modal pattern of seasonal variations of TLR is in contrast to results from other mountain regions. Results also show a different controlling factor on the magnitude of TLRs for individual seasons.

The winter season is dominated by clear skies and negligible precipitation, leading to strong nighttime cooling with down-slope cold airflow and subsequent deposition in valleys and low-elevation areas. Fog may also enhance the temperature inversion in winter. These topographic and inversion effects result in the lowest TLR in winter, particularly during the nighttime. Contrastingly, summer experiences the heaviest rainfall and largest cloud cover. Heavy rainfall is associated with latent heat release due to vapor condensation, which is used to heat the air over higher elevations. Increased cloud cover decreases the surface temperature by reflecting solar radiation during the day. These conditions contribute to the second lowest value of TLR in summer, particularly during the daytime.

The highest TLR is found during the pre-monsoon season associated with generally clear skies. This season also has the largest difference between maximum and minimum TLR. This difference may be associated with strong dry convection during the day and strong radiative cooling at night in the absence of clouds. A second peak in TLR is found during the post-monsoon season. The weather conditions during this time are similar those in the pre-monsoon season, but with relatively wet land surfaces after the summer rainfall. Consequently, the TLR values during the post-monsoon season are similar to those during the pre-monsoon season, but with a smaller magnitude.

Acknowledgments The National Natural Science Foundation of China (Grants No. 41190081, 40830638 and 40810019001) and the Chinese Academy of Sciences Third Pole Environment Program (GJHZ 0906) supported this work. The authors thank the Department of Hydrology and Meteorology, Government of Nepal for providing the data. We also thank Dr. Gareth Hearn, the editor, and the anonymous reviewer for providing valuable comments to revise this paper and Meri Joswiak for assistance with English editing.

References

Barry RG (2002) Mountain climate change and cryospheric: a review. In: Berger T. et al. (eds). Mountain of the world. Proceedings of the World Mountain Symposium (WMS 2001), Swiss Agency for Development and Cooperation, Bern, Switzerland

Barry RG, Chorley RJ (2003) Atmosphere, weather and climate, 8th edition (1st edition 1968). Routledge, London, p 25

Bhutiyani MR, Kale VS, Pawar NJ (2007) Long term trends in maximum, minimum and mean annual temperatures across the northwestern Himalaya during the twentieth century. Clim Chang 85:159–177

Blandford TR, Humes KS, Harshburger BJ, Moore BC, Walden VP, Ye H (2008) Seasonal and synoptic variations in near-surface air temperature lapse rates in a mountainous basin. J Applied Meteorol Climatol 47:249–261. doi:10.1175/2007JAMC1565.1

Critchfield HJ (2004) General climatology, 4th edition (1st edition 1983). Prentice-Hall, New Delhi

Devkota LP (2004) Climate variability over Nepal: observations, forecasting, model evaluation and impacts on agriculture and water resources. Dissertation, Tribhuvan University, Nepal.

Diaz HF, Bradley RS (1997) Temperature variations during the last century at high elevation sites. Clim Chang 36:253–279. doi:10.1023/A:1005335731187

Dimri AP (2007) The transport of momentum, sensible heat, potential energy and moisture over the western Himalayas during the winter season. Theor Appl Climatol 90:49–63. doi:10.1007/s00704-006-0274-0

Dobrowski SZ, Abatzoglou JT, Greenberg JA, Schladow SG (2009) How much influence does landscape-scale physiography have on air temperature in a mountain environment? Agric For Meteorol 149:1751–1758

Flohn H (1957) Large-scale aspects of the "summer monsoon" in south and east Asia. J Meteorol Soc Jpn 35:180–186

Flohn H (1968) Contribution to meteorology of the Tibetan Highland. Atmospheric Science Paper No. 130. Colorado University, Fort Collins, 1080523

Gardner AS, Sharp MJ, Koerner RM, Labine C, Boon S, Marshall SJ, Burgess DO, Lewis D (2009) Near-surface temperature lapse rates over Arctic Glaciers and their implications for temperature downscaling. J Clim 22(16):4281–4298

Gouvas MA, Sakellariou NK, Kambezidis HD (2011) Estimation of the monthly and annual mean maximum and mean minimum air temperature values in Greece. Meteorol Atmos Phys 110:143–149

Grubbs FE (1950) Sample criteria for testing outlying observations. Ann Math Stat 21:27–58

Grubbs FE (1969) Procedures for detecting outlying observations in samples. Technometrics 11(1):13–14

Harlow RC, Burke EJ, Scott RL, Shuttleworth WJ, Brown CM, Petti JR (2004) Derivation of temperature lapse rates in semi-arid south-eastern Arizona. Hydrol Earth Syst Sci 8(6):1179–1185

Ichiyanagi K, Yamanaka MD, Muraji Y, Vaidya BK (2007) Precipitation in Nepal between 1987 and 1996. Int J Climatol 27:1753–1762. doi:10.1002/joc.1492

Kansakar SL, Hannah DM, Gerrard J, Ress G (2004) Spatial pattern in the precipitation regime of Nepal. Int J Climatol 24:1645–1659

Kurosaki Y, Kimura F (2002) Relationship between topography and daytime cloud activity around Tibetan Plateau. J Meteor Soc Japan 80:1339–1355

Lang TJ, Barros AP (2002) An investigation of the onsets of the 1999 and 2000 monsoons in Central Nepal. Mon Weather Rev 131:1408–1427

Laughlin GP (1982) Minimum temperature and lapse rate in complex terrain: Influencing factors and prediction. Arch Met Geoph Biokl Ser B 30:141–152

Marshall SJ, Sharp MJ, Burgess DO, Anslow FS (2007) Near-surface-temperature lapse rates on the Prince of Walse Icefield, Ellesmere Island, Canada: Implications for regional downscaling of temperature. Int J Climatol 27:385–398. doi:10.1002/joc.1396

Minder JR, Mote PW, Lundquist JD (2010) Surface temperature lapse rates over complex terrain: lessons from the Cascade Mountains. J Geophys Res 115:D14122. doi:10.1029/2009JD013493

Mokhov II, Akperov MG (2006) Tropospheric lapse rate and its relation to surface temperature from reanalysis data. Izvestiya Atmos Ocean Phys 42(4):430–438. doi:10.1134/S0001433806040037

Pepin N (2001) Lapse rate changes in Northern England. Theor Appl Climatol 68:1–16

Pepin N, Losleben M (2002) Climate change in the Colorado Rocky Mountains: free air versus surface temperature trends. Int J Climatol 22:311–392

Richardson AD, Lee X, Friedland AJ (2004) Microclimatology of tree line spruce–fir forests in mountains of the northeastern United States. Agric For Meteorol 125:53–66

Rolland C (2003) Spatial and seasonal variations of air temperature lapse rates in Alpine regions. J Clim 16:1032–1046

Shrestha ML (2000) Inter annual variation of summer monsoon rainfall over Nepal and its relation to Southern Oscillation Index. Meteorol Atmos Phys 75:21–28

Shrestha AB, Aryal R (2010) Climate change in Nepal and its impact on Himalayan glacier. Reg Environ Change. doi:10.1007/s10113-010-0174-9

Shrestha AB, Wake CP, Dibb JE, Mayewski PA (2000) Precipitation fluctuations in the Nepal Himalaya and its vicinity and relationship with some large scale. Int J Climatol 20:317–327

Stone PH, Carlson JH (1979) Atmospheric lapse rate regimes and their parameterization. J Atmos Sci 36:415–423

Tang Z, Fang J (2006) Temperature variation along the northern and southern slopes of Mt. Taibai, China. Agric For Meteorol 139:200–207

Tetens O (1930) Uber einige meteorologische begrie. Z Geo-physics 6:297–309

Thyer N (1985) Looking at western Nepal's climate. Bull Am Meteorol Soc 66(6):645–650

Ueno K, Toyotsu K, Bertolani L, Tartari G (2008) Stepwise onset of monsoon weather observed in the Nepal Himalaya. Mon Weather Rev 136:2507–2522. doi:10.1175/2007MWR2298.1

Wu G, Zhang Y (1998) Tibetan Plateau forcing and timing of the monsoon onset over South Asia and South China Sea. Mon Wea Rev 126:913–927

Yang K, Ye B, Zhou D, Wu B, Foken T, Qin J, Zhou Z (2011) Response of hydrological cycle to recent climate changes in the Tibetan Plateau. Clim Chang 109:517–534. doi:10.1007/s10584-011-0099-4

Yao T, Pu J, Lu A, Wang Y, Wusheng Y (2006) Recent glacial retreat and its impact on Hydrological processes on the Tibetan Plateau, China, and surrounding regions. Arct Antarct Alp Res 39(4):642–650

Ye D, Gao Y (1979) The meteorology of the Qinghai-Xizang (Tibet) Plateau (in Chinese). Science Press, Beijing, 278 pp